Hindawi
Journal of Sensors
Volume 2019, Article ID 5345901, 6 pages
https://doi.org/10.1155/2019/5345901

Research Article

Measurement of Mechanical and Thermal Strains by Optical FBG Sensors Embedded in CFRP Rod

Keunhee Cho, Sung Tae Kim, Young-Hwan Park, and Jeong-Rae Cho

Department of Infrastructure Safety Research, Korea Institute of Civil Engineering and Building Technology, Goyang-Si 10223, Republic of Korea

Correspondence should be addressed to Jeong-Rae Cho; chojr@kict.re.kr

Received 17 May 2019; Revised 29 July 2019; Accepted 23 August 2019; Published 8 October 2019

Academic Editor: Carlos Marques

The present study intends to provide the photoelastic coefficient and thermal expansion coefficient needed to use an FBG-embedded CFRP rod (smart rod) as strain sensor. Due to the monolithic combination of the FBG sensor with a CFRP rod, the smart rod is likely to exhibit thermal and mechanical properties differing from those of the bare FBG sensor. A tensile test showed that the photoelastic coefficient of the smart rod is 0.204, which is about 7.3% lower than the 0.22 value of the bare optical FBG. Moreover, the thermal expansion coefficient of the smart rod obtained through a thermal test appeared to be negative with a low value of $-0.190 \times 10^{-6}/^{\circ}\mathrm{C}$. Consequently, the temperature dependence of the smart rod is mainly expressed by means of the thermooptic coefficient. Compared to the bare FBG sensor, the smart rod is easier to handle and can measure compressive strains, which make it a convenient sensor for various concrete structures.

1. Introduction

FBG (fibre Bragg grating) sensors are widely used in telecommunication and measurement [1]. It is basically used as a strain sensor and for expanding the application area, and it can be used for the measurement of acceleration [2] and liquid level [3], temperature field detection using a linearly chirped FBG [4], and biodetection using an SPR (surface plasmon resonance) sensor [5]. There is also a smart rod [6] that has been developed to easily install FBG sensors on concrete structures.

Because bare fibre is weak in shear, folding, etc., very careful handling is required to apply it to a concrete structure. A FBG-embedded CFRP rod (smart rod, thereafter) is proposed to solve these problems, which provides extra protection for the optical fibre and also perfect bondage between the sensor and concrete [6]. This smart rod was utilized to measure the prestress force in a PSC (prestressed concrete) structure by disposing the smart rod instead of the core wire of the strand [7, 8]. The smart rod thus played both the roles of the sensor and the core wire of the strand. Figure 1 shows the appearance of the smart rod with an 80% volume fraction of carbon fibre and an epoxy matrix. The jacket was applied only to the part for extracting the optical fibre, and the jacket was not applied to the remaining part. Therefore, there is no jacket at the FBG position, and the optical fibre behaves monolithically with the CFRP rod.

Due to the monolithic combination of the sensor with CFRP, the smart rod exhibits thermal and mechanical properties differing from those of the bare fibre optic sensor [9]. This implies that the various formulae and constants proposed to convert the wavelength measured by the bare fibre optic sensor into strain and temperature data cannot be applied readily.

Magne et al. [10] proposed the following basic formula for the bare optical FBG:

$$\frac{\Delta\lambda}{\lambda_B} = (1 - p_e)\epsilon_m + (\alpha_f + \xi)\Delta T, \tag{1}$$

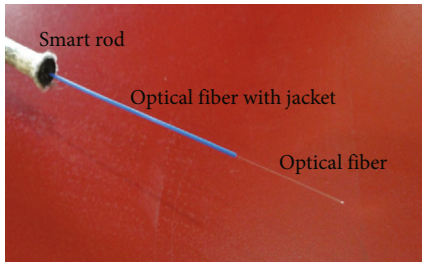

Figure 1: Appearance of the smart rod.

where λ_B = central Bragg wavelength; $\Delta\lambda$ = wavelength shift; p_e = photoelastic coefficient (0.22 for optical fibre made of SiO_2); ϵ_m = mechanical strain; α_f = thermal expansion coefficient; ξ = thermooptic coefficient; and, ΔT = thermal gradient.

However, this formula cannot be adopted as expressed in equation (1) when the fibre optic sensor is bonded to a matrix or host material. In such case, the modified formulae in equations (2) and (3) are used.

$$\frac{\Delta\lambda}{\lambda_B} = (1-p_e)\epsilon_m + \left[(\alpha_f+\xi) + (1-p_e)(\alpha_h-\alpha_f)\right]\Delta T, \quad (2)$$

$$\frac{\Delta\lambda}{\lambda_B} = (1-p_e)\epsilon_m + [\xi + (1-p_e)\alpha_h]\Delta T, \quad (3)$$

where α_h = thermal expansion coefficient of the host material.

Equation (2) is an implicit formula that can be applied when the fibre optic sensor is bonded to the host material [10]. Equation (3) corresponds to equation (2) where the thermal expansion coefficient of the fibre optic sensor ($\alpha_f = 0.5\times10^{-6}/°C$ for the fiber optic sensor made of SiO_2) is ignored [11, 12]. With the thermal expansion coefficient being very low, these two formulas provide similar results.

The smart rod realizes the perfect monolithic combination of the optical fiber with the CFRP rod by being fabricated through the concurrent pultrusion of the carbon fiber and the optical fiber. Therefore, the photoelastic coefficient of the smart rod differs from that of the bare optical fiber [9]. In addition, knowing the thermal expansion coefficient of the smart rod is also necessary to obtain the thermal strain or to perform the temperature calibration. The present study intends to suggest coefficients fitted to the smart rod for its use as a strain sensor. Section 2 presents the derivation of the photoelastic coefficient of the smart rod, and Section 3 proposes the derivation of the thermal expansion coefficient for the smart rod.

2. Photoelastic Coefficient of the Smart Rod

In the absence of a temperature gradient, the relation between the wavelength and the strain can be expressed as

$$\frac{\Delta\lambda}{\lambda_B} = (1-p_e)\epsilon_m, \quad (4)$$

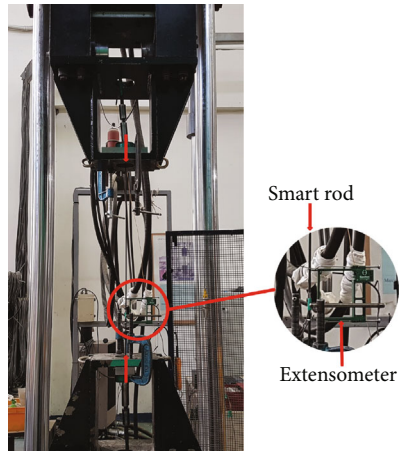

Figure 2: Tensile test of the smart rod.

where the photoelastic coefficient, p_e, is defined as follows [13]:

$$p_e = \frac{n^2}{2}[p_{12} - \nu(p_{11}+p_{12})], \quad (5)$$

where n = refractive index of optical fibre; p_{11}, p_{12} = Pockel's coefficients; and ν = Poisson's ratio.

The refractive index and Pockel's coefficients are independent of the eventual bond or composition between the optical fibre and the host material. Besides, Poisson's ratio takes values different from that of the bare optical fibre according to the extent by which the optical fibre is bonded or composed with the host material. This means that the smart rod will have a photoelastic coefficient different from that of the bare optical fibre.

Figure 2 depicts the tensile test conducted to derive the photoelastic coefficient of the smart rod. The smart rod was gripped at its ends and subjected to tension using an actuator. The wavelength was measured by an interrogator, and the change in strain was obtained by converting the corresponding relative strain measured by an extensometer. Four specimens were tested. The first specimen was used for the experimental setting, and data were acquired using the remaining 3 specimens.

Rearranging equation (4) in terms of the mechanical strain gives equation (6). Figure 3 plots the wavelength and strain measured in each specimen. The experimental wavelength and strain confirm the linear relationship between the wavelength and the strain as expressed in

$$\epsilon_m = \frac{\lambda-\lambda_0}{\lambda_B(1-p_e)} \approx \frac{\lambda-\lambda_0}{\lambda_0(1-p_e)}, \quad (6)$$

where λ_0 = initial wavelength. Since there is practically no difference between the central Bragg wavelength λ_B and the initial wavelength λ_0, λ_B can be replaced by λ_0 [12].

Because the strain ϵ_m of the FBG sensor in equation (6) must be equal to the strain ϵ_{ext} of the extensometer, the minimization problem expressed in equation (7) can

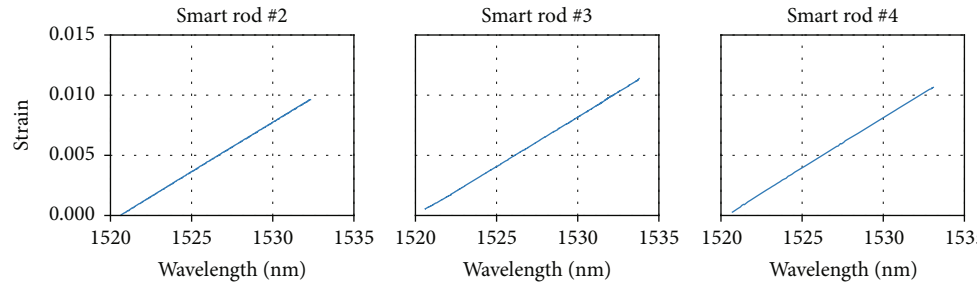

Figure 3: Relation between the wavelength of the smart rod and the strain of the extensometer.

Table 1: Photoelastic coefficients of smart rod specimens.

	p_e
Smart rod #2	0.200
Smart rod #3	0.201
Smart rod #4	0.211
Average	0.204

be formulated for each specimen. Since ϵ_m is a linear equation of wavelength, it can be set to $\epsilon_m = m\lambda + c$, where $m = 1/\lambda_0(1 - p_e)$ and $c = -1/(1 - p_e)$. Solving equation (7) by the least square method can obtain m and c, and p_e and λ_0 can be obtained from it. Solving this minimization problem for each specimen gives the photoelastic coefficients listed in Table 1. The strain of the FBG obtained by applying these photoelastic coefficients is compared to the strain provided by the extensometer in Figure 4.

$$\min |\epsilon_m - \epsilon_{\text{ext}}| = \min |(m\lambda + c) - \epsilon_{\text{ext}}|. \tag{7}$$

The comparison in Figure 4 confirms the good agreement between the strains obtained from the smart rod and the extensometer and that the minimization problem was also well solved. In addition, R^2 is close to 1 in all three specimens, so the measurement error in the experiment is very small. The values in Table 1 reveal that the photoelastic coefficients of the smart rod specimens range between 0.200 and 0.211 with an average of 0.204, which represents a difference of about 7.3% compared to the value of 0.22 known for the bare optical fibre. This difference in the photoelastic coefficient results in a strain difference of approximately 2%, which cannot be disregarded in terms of sensing performance.

3. Thermal Expansion Coefficient of the Smart Rod

If a temperature gradient occurs in a no-stress state, the relationship between the wavelength and the strain change can be derived as equations (8) and (9) from equation (1) for the bare optical FBG and equation (2) for the smart rod, respectively.

$$\frac{\Delta\lambda}{\lambda_B} = a\Delta T, \tag{8}$$

where $a = \alpha_f + \xi$, and

$$\frac{\Delta\lambda}{\lambda_B} = b\Delta T, \tag{9}$$

where $b = (\alpha_f + \xi) + (1 - p_e)(\alpha_h - \alpha_f)$.

With the thermal expansion coefficient α_f being $0.5 \times 10^{-6}/°\text{C}$ for the bare optical fibre made of SiO_2, the unknowns in equations (8) and (9) are the thermooptic coefficient ξ and the thermal expansion coefficient α_h of the host material. As shown in Figure 5, a temperature test was performed on the bare optical fibre and the smart rod in order to determine the thermooptic coefficient ξ of the smart rod and the thermal expansion coefficient α_h of the material hosting the FBG in the smart rod. In the test, 3 sets of bare fibre and smart rod in a no-stress state were subjected to thermal loading running from −15°C to 55°C.

Figure 6 plots the time histories of the temperature and wavelengths of the bare optical FBR and smart rod recorded in the third test (Trial #3). Figure 7, which redraws these time histories in terms of the temperature versus $\Delta\lambda/\lambda_B$, shows the linear relation between the two variables. In addition, R^2 values are close to 1, so the measurement error in the experiment is very small. Figure 8 presents the linear regression for the measured time histories. The results of Trial #1 and Trial #2 arranged through the same process are listed in Table 2. In Table 2, a and b are the slopes of the linear regression lines of the bare optical FBG and smart rod in Figure 8. These two constants can be used to calculate the thermooptic coefficient and thermal expansion coefficient of the host material by simple arithmetic.

The so-obtained thermooptic coefficient ξ and thermal expansion coefficient α_h for the smart rod are $5.439 \times 10^{-6}/°\text{C}$ and $-0.190 \times 10^{-6}/°\text{C}$, respectively. The negative value calculated for the thermal expansion coefficient is noteworthy and can be attributed to the properties of CFRP of which the representative range of the thermal expansion coefficient is $-9.0 \sim 0.0 \times 10^{-6}/°\text{C}$ [14]. Considering the small values of the thermal expansion coefficient of the bare optical fibre and smart rod, the temperature dependence of the smart rod can be accounted by means of the thermooptic coefficient. Moreover, the smart rod appears to be less dependent to temperature than the bare optical fibre.

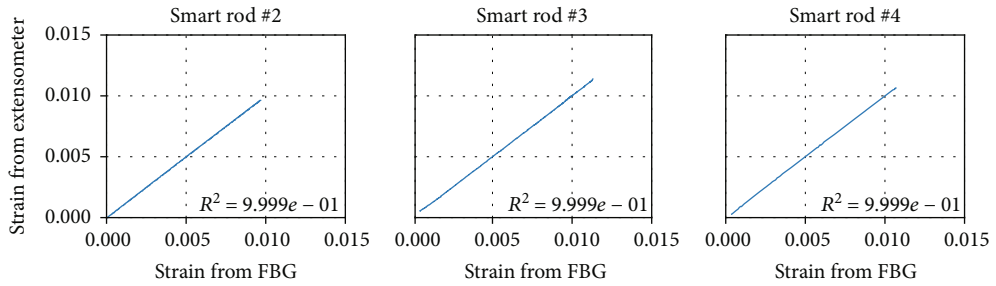

Figure 4: Comparison of strains obtained from the smart rod and the extensometer.

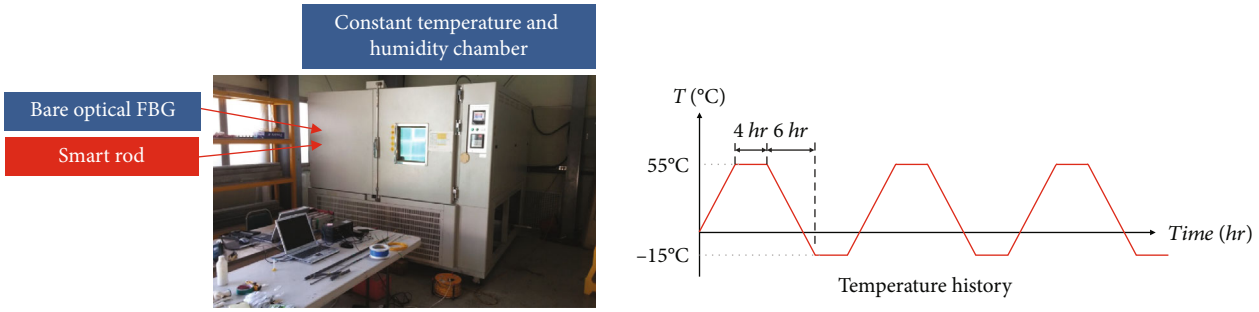

Figure 5: Test for the determination of temperature-related coefficients.

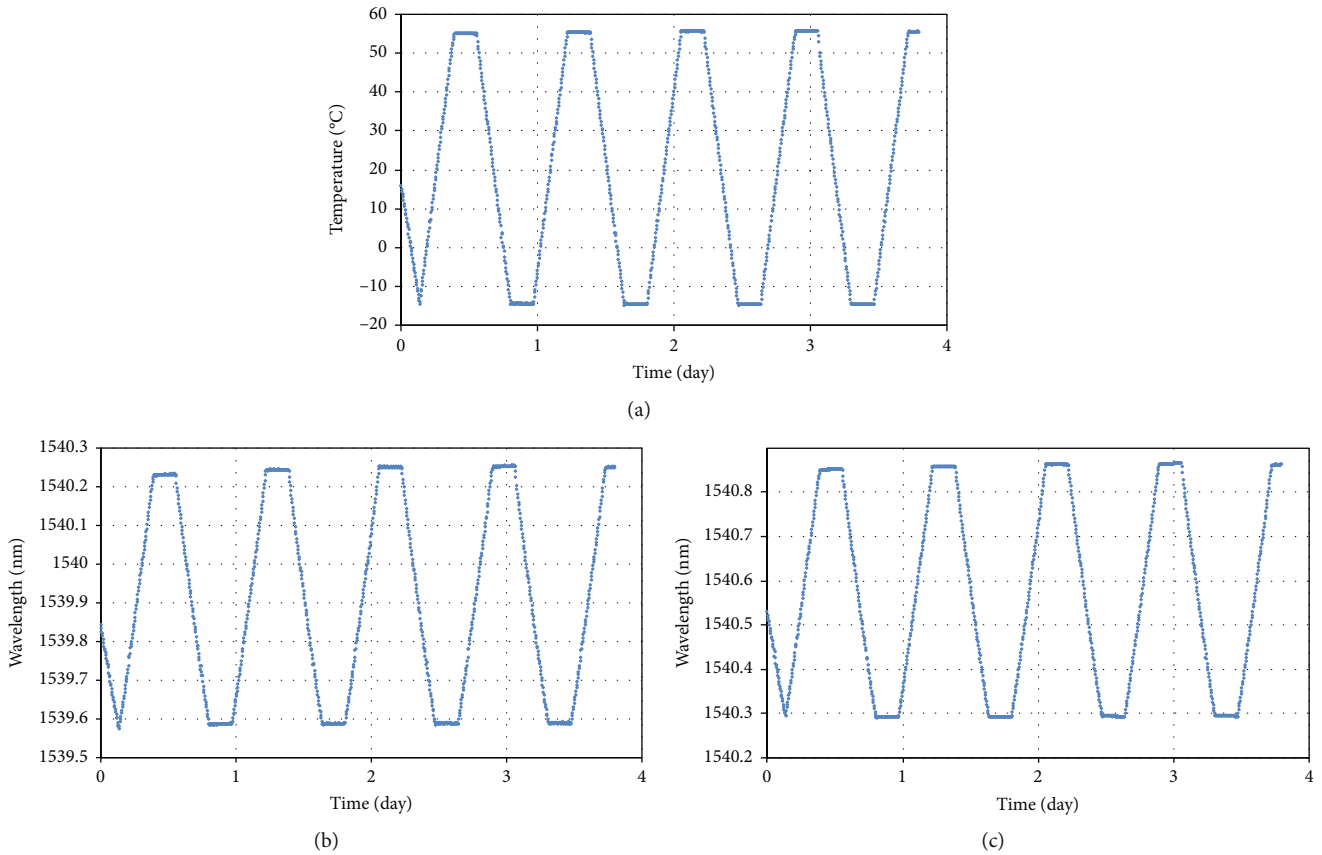

Figure 6: Time histories of (a) temperature, (b) wavelength of bare optical FBG, and (c) wavelength of the smart rod measured in Trial #3.

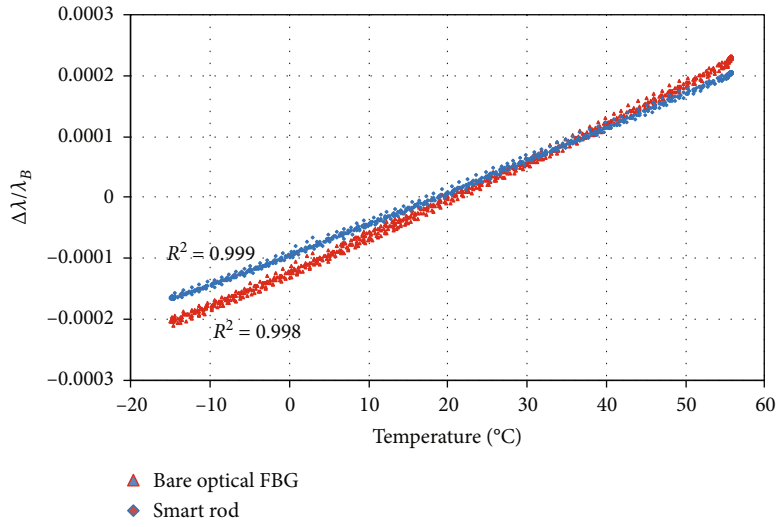

Figure 7: Temperature-$\Delta\lambda/\lambda_B$ curves derived from experimental data of Trial #3.

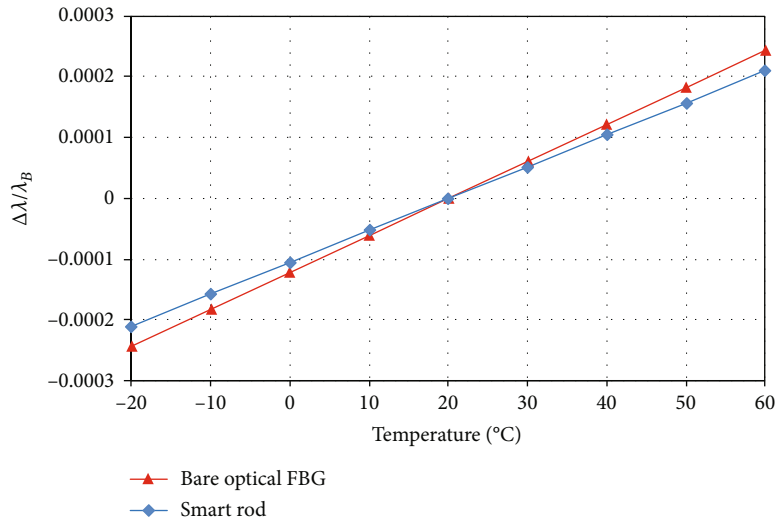

Figure 8: Linear regression of temperature-$\Delta\lambda/\lambda_B$ curves from Trial #3.

Table 2: Test results and thermooptic coefficient and thermal expansion coefficient of the host material.

	Test results		Determined constants	
	a $(\times 10^{-6}/°C)$	b $(\times 10^{-6}/°C)$	ξ $(\times 10^{-6}/°C)$	α_h $(\times 10^{-6}/°C)$
Trial #1	5.931	5.554	5.431	0.016
Trial #2	6.084	5.239	5.584	-0.380
Trial #3	5.803	5.378	5.303	-0.205
Average	5.939	5.390	5.439	-0.190

4. Conclusions

This paper determined experimentally the photoelastic coefficient and thermal expansion coefficient of the smart rod that are necessary for its use as a strain sensor. Due to the concurrent pultrusion of the bare optical fibre and CFRP applied to fabricate it, the smart rod exhibits the perfect composition of both components. This implies that the smart rod develops not only thermal but also photoelastic properties differing from those of the bare optical fibre. The photoelastic coefficient of the smart rod determined from the tensile test reached 0.204, which differs by about 7.3% compared to the value of 0.22 for the bare optical fibre, and the thermal expansion coefficient of the smart rod obtained from temperature test was negative with a low value of $-0.190 \times 10^{-6}/°C$. Accordingly, the temperature dependence of the smart rod can be expressed exclusively by means of the thermooptic coefficient. Compared to the bare optical fibre, the smart rod is easier to handle and can measure compressive strains that makes it a convenient sensor for various structures.

Data Availability

The data used to support the findings of this study are available from the corresponding author upon request.

Conflicts of Interest

The authors declare that there is no conflict of interest regarding the publication of this paper.

Acknowledgments

This research was funded by the Korea Institute of Civil Engineering and Building Technology through a grant from a Strategic Research Project (Smart Monitoring System for Concrete Structures Using FRP Nerve Sensor).

References

[1] A. Othonos and K. Kalli, *Fiber Bragg Gratings, Fundamentals and Applications in Telecommunications and Sensing*, Artech House Publishing, Norwood, MA, USA, 1999.

[2] P. F. C. Antunes, C. A. Marques, H. Varum, and P. S. Andre, "Biaxial optical accelerometer and high-angle inclinometer with temperature and cross-axis insensitivity," *IEEE Sensors Journal*, vol. 12, no. 7, pp. 2399–2406, 2012.

[3] C. A. R. Diaz, A. G. Leal-Junior, P. S. B. Andre et al., "Liquid level measurement based on FBG-embedded diaphragms with temperature compensation," *IEEE Sensors Journal*, vol. 18, no. 1, pp. 193–200, 2018.

[4] S. Korganbayev, R. Min, M. Jelbuldina et al., "Thermal profile detection through high-sensitivity fiber optic chirped Bragg grating on microstructured PMMA fiber," *Journal of Lightwave Technology*, vol. 36, no. 20, pp. 4723–4729, 2018.

[5] C. Caucheteur, Y. Shevchenko, L.-Y. Shao, M. Wuilpart, and J. Albert, "High resolution interrogation of tilted fiber grating SPR sensors from polarization properties measurement," *Optics Express*, vol. 19, no. 2, pp. 1656–1664, 2011.

[6] S. Kim, Y. H. Park, S. Park, K. Cho, and J. R. Cho, "A sensor-type PC strand with an embedded FBG sensor for monitoring prestress forces," *Sensors*, vol. 15, no. 1, pp. 1060–1070, 2015.

[7] K. Cho, S. Kim, J.-R. Cho, and Y.-H. Park, "Analytical model of nonlinear stress-strain relation for a strand made of two materials," *Materials*, vol. 10, no. 9, p. 1003, 2017.

[8] K. Cho, S. Kim, J.-R. Cho, and Y.-H. Park, "Estimation of tendon force distribution in prestressed concrete girders using smart strand," *Applied Sciences*, vol. 7, no. 12, p. 1319, 2017.

[9] V. P. Matveenko, I. N. Shardakov, A. A. Voronkov et al., "Measurement of strains by optical fiber Bragg grating sensors embedded into polymer composite material," *Structural Control and Health Monitoring*, vol. 25, no. 3, article e2118, 2018.

[10] S. Magne, S. Rougeault, M. Vilela, and P. Ferdinand, "State-of-strain evaluation with fiber Bragg grating rosettes: application to discrimination between strain and temperature effects in fiber sensors," *Applied Optics*, vol. 36, no. 36, pp. 9437–9447, 1997.

[11] G. Pereira, M. McGugan, and L. P. Mikkelsen, "Method for independent strain and temperature measurement in polymeric tensile test specimen using embedded FBG sensors," *Polymer Testing*, vol. 50, pp. 125–134, 2016.

[12] M. Kreuzer, *Strain Measurement with Fiber Bragg Grating Sensors*, HBM, Darmstadt, Germany, 2006.

[13] C. D. Butter and G. B. Hocker, "Fiber optics strain gauge," *Applied Optics*, vol. 17, no. 18, pp. 2867–2869, 1978.

[14] ACI, *Guide for the Design and Construction of Structural Concrete Reinforced with Fiber-Reinforced Polymer (FRP) Bars*, ACI, Farmington Hills, MI, USA, 2015.